

# A solar-type star polluted by calcium-rich supernova ejecta inside the supernova remnant RCW 86

Vasilii V. Gvaramadze<sup>1,2,3,\*</sup>, Norbert Langer<sup>4</sup>, Luca Fossati<sup>5</sup>, Douglas C.-J. Bock<sup>6</sup>, Norberto Castro<sup>4,7</sup>, Iskren Y. Georgiev<sup>8</sup>, Jochen Greiner<sup>9</sup>, Simon Johnston<sup>6</sup>, Arne Rau<sup>9</sup> & Thomas M. Tauris<sup>10,4</sup>

Received ; Accepted ; published online by Nature on . DOI:

<sup>1</sup>*Sternberg Astronomical Institute, Lomonosov Moscow State University, Universitetskij Pr. 13, Moscow 119992, Russia*

<sup>2</sup>*Space Research Institute, Russian Academy of Sciences, Profsoyuznaya 84/32, 117997 Moscow, Russia*

<sup>3</sup>*Isaac Newton Institute of Chile, Moscow Branch, Universitetskij Pr. 13, Moscow 119992, Russia*

<sup>4</sup>*Argelander-Institut für Astronomie, Auf dem Hügel 71, 53121 Bonn, Germany*

<sup>5</sup>*Space Research Institute, Austrian Academy of Sciences, Schmiedlstrasse 6, 8042 Graz, Austria*

<sup>6</sup>*CSIRO Astronomy and Space Science, Australia Telescope National Facility, PO Box 76, Epping, NSW 1710, Australia*

<sup>7</sup>*Department of Astronomy, University of Michigan, 1085 S. University Avenue, Ann Arbor, MI 48109, USA*

<sup>8</sup>*Max-Planck Institut für Astronomie, Königstuhl 17, 69117 Heidelberg, Germany*

<sup>9</sup>*Max-Planck-Institut für extraterrestrische Physik, Giessenbachstr. 1, 85748 Garching, Germany*

<sup>10</sup>*Max-Planck-Institut für Radioastronomie, Auf dem Hügel 69, 53121 Bonn, Germany*

**When a massive star in a binary system explodes as a supernova its companion star may be polluted with heavy elements from the supernova ejecta. Such a pollution had been detected in a handful of post-supernova binaries<sup>1</sup>, but none of them is associated with a supernova remnant. We report the discovery of a solar-type star in a close, eccentric binary system with a neutron star within the young Galactic supernova remnant RCW 86. Our discovery implies that the supernova progenitor was a moving star, which exploded near the edge of its wind bubble and lost most of its initial mass due to common-envelope evolution shortly before core collapse. We find that the solar-type star is strongly polluted with calcium and other elements, which places the explosion within the class of calcium-rich supernovae – faint and fast transients<sup>2,3</sup>, whose origin is strongly debated<sup>4,5</sup>, and provides the first observational evidence that supernovae of this type can arise from core-collapse explosions<sup>4,6</sup>.**

Recently, it was recognized that a large fraction of massive stars reside in binary systems<sup>7,8</sup> and that the evolution of the majority of massive stars is strongly affected by binary interaction, through mass transfer, common envelope evolution or merger<sup>7</sup>. This suggests that most Type Ib/c supernovae (SNe), which do not show hydrogen lines in their spectra, stem from progenitors which are stripped of their hydrogen envelopes by a companion star<sup>9,10</sup>. The low ejecta masses typical of such SNe<sup>11</sup> imply that a significant fraction of the post-SN binaries remain bound. Only very few of such binaries are known<sup>12,13</sup> to be associated with supernova remnants (SNRs) because of the short lifetime ( $\sim 10^5$  yr) of the SNRs. In this Letter, we report the discovery of a post-SN binary

system within the young (few thousand years<sup>14</sup>) SNR RCW 86.

The pyriform appearance of RCW 86 (Fig. 1; see also fig. 6 in ref.<sup>16</sup>) can be explained as the result of a SN explosion near the edge of a bubble blown by the wind of a moving massive star<sup>17,18</sup> (Supplementary Information section 1). This interpretation implies that the SN exploded near the centre of the hemispherical optical nebula in the south-west of RCW 86 (see Fig. 1) and that the stellar remnant should still be there. Motivated by these arguments, we looked for a possible compact X-ray source using archival *Chandra* data and discovered<sup>17</sup> two sources in the expected position of the SN progenitor (Fig. 1). One of them, [GV2003] S, has a clear optical counterpart with  $V=14.4$  mag and its X-ray spectrum implies that this source is a foreground late-type active star. For the second source, [GV2003] N, we did not find any optical counterpart in the Digital Sky Survey II to a limiting red band magnitude of  $\approx 21$ , while its X-ray spectrum suggests that this source could be a young pulsar<sup>17</sup>. Our deep follow-up observation with the Parkes radio telescope in 2002, however, failed to detect any radio emission from [GV2003] N, giving an upper limit on the flux of  $35 \mu\text{Jy}$  at 1420 MHz (see Methods). This non-detection may be a consequence of beaming or it could indicate that [GV2003] N may not be an active radio pulsar.

If [GV2003] N was a NS its emission in the visual was expected to be fainter than  $V \approx 28$  mag. We therefore obtained a  $V$ -band image of the field around this source with the FORS2 instrument on the ESO Very Large Telescope (VLT) in 2010. The FORS2 image, however, revealed a stellar-like object with  $V=20.69 \pm 0.02$  mag just at the position of [GV2003] N (Fig. 1; Methods). To further constrain the nature of [GV2003] N, we obtained its  $g'r'i'z'JHK_s$  photometry with the 7-channel optical/near-infrared imager GROND in 2013 (Methods). With that, we fitted the spectral energy distribution (SED) of [GV2003] N and derived a temperature of  $\approx 5200$  K and a colour excess of  $E(B-V) \approx 0.9$  mag (Methods; Extended Data Fig. 1). These results exclude the possibility that [GV2003] N is an AGN (as it was proposed in ref.<sup>19</sup>) and strongly suggest that the optical emission originates from a G-type star at a distance comparable to that of RCW 86 of  $2.3 \pm 0.2$  kpc<sup>20</sup>. Since the X-ray luminosity of [GV2003] N of  $\sim 10^{32} \text{ erg s}^{-1}$  (ref.<sup>17,19</sup>) is far too high for a G star<sup>21</sup>, we arrived at the possibility that we are dealing with a G star orbiting the NS.

Consequently, we searched for radial velocity (RV) variability and traces of the SN ejecta in the spectrum of the optical counterpart of [GV2003] N. We obtained four spectra with the VLT/FORS2 in 2015. We found clear RV variations (Table 1), indicative of an eccentric binary with a period of about a month or less (Methods). The spectrum of [GV2003] N (Fig. 2) clearly resembles that of a solar-type star, confirming the results from the SED analysis.

From the analysis of the Fe I lines (Methods), we derived a stellar effective temperature of  $T_{\text{eff}} = 5100 \pm 200$  K. Using  $V=20.69$  mag,  $E(B-V)=0.9$  mag and assuming the ratio of total to selective extinction of  $R_V=3.1$ , we estimated a visual extinction and absolute magnitude of  $A_V=2.79$  mag and  $M_V=6.09$  mag, respectively. With a bolometric correction of  $-0.29$  mag<sup>22</sup>, we obtained a bolometric luminosity of  $\log(L/L_\odot) = -0.42 \pm 0.08$ , taking into account the uncertainty on the distance. Using the Pisa stellar models<sup>23</sup>, we estimated the mass of the optical star as  $\approx 0.9 M_\odot$ , which for the given  $T_{\text{eff}}$  and  $L$  corresponds to a surface gravity of  $4.6 \pm 0.1$ . The fact that the binary system remained bound after the SN explosion, and assuming the standard mass of a NS of

1.4  $M_{\odot}$ , implies a mass of the SN ejecta of less than 2.3  $M_{\odot}$  — provided that the SN explosion was symmetric<sup>24</sup> — and a mass of the exploding star below 3.7  $M_{\odot}$ . This in turn implies that the SN explosion was of Type Ib and that the initial mass of the primary star was smaller than 13  $M_{\odot}$ <sup>25</sup>.

From the FORS2 spectra we derived the abundances of Si, Ca, Ti, V, Cr, Mn, Fe, Co, Ni, and Ba (Methods). Fig. 3 shows that many elements are enhanced by a factor of about 3 with respect to the solar abundances<sup>26</sup>, with the silicon and iron being less than doubled. Calcium is particularly overabundant, by a factor of  $\approx 6$ , which, to our knowledge, makes [GV2003] N the most Ca-rich star known to date.

The SN ejecta captured by the G star are mixed with the material of its convective envelope. Adopting an envelope mass of 0.2  $M_{\odot}$ <sup>27</sup>, we computed the mass accreted from the SN ejecta for each element with measured abundances (Extended Data Table 1), which sums up to  $3.3 \times 10^{-4} M_{\odot}$ . Since the accreted mass of iron of  $\approx 1.5 \times 10^{-4} M_{\odot}$  was ejected in the form of  $^{56}\text{Ni}$ , an accreted fraction of the SN ejecta of about 1% would lead to a total mass of radioactive nickel produced by the SN of 0.015  $M_{\odot}$ . These numbers appear consistent, since the explosion energy of SNe of  $\sim 10 M_{\odot}$  stars is thought to be low, with the consequence of a relatively low nickel mass and moderate ejecta velocities<sup>28</sup>, allowing for a rather high accreted fraction of the SN ejecta (Supplementary Information section 4).

The large amount of Ca in [GV2003] N, together with the rather modest enhancement of Si suggest that the SN, which produced RCW 86, was not a typical core-collapse event (Supplementary Information section 2). Instead, our data suggest that it belonged to the class of Ca-rich SNe — the fast and faint transients, which show strong Ca lines in their spectra and are believed to be intrinsically calcium-rich<sup>29</sup> (Supplementary Information section 3). Whereas observations indicate that many of the Ca-rich SNe are produced by long-lived low-mass stars, our findings imply that the lowest mass stars capable of producing NSs can produce similar explosion, if the progenitor is stripped of its envelope by a companion star. Indeed, from theoretical considerations, in both cases the explosion is produced in a helium layer with an inner radius comparable to that of a white dwarf, and an explosion kinetic energy of less than  $10^{51}$  erg (Supplementary Information section 3).

The short orbital period of [GV2003] N implies that this binary system will evolve into a low-mass X-ray binary (LMXB) within its nuclear time scale ( $\sim 10^{10}$  yr), providing the first definite example of a pre-LMXB located within a SNR. Before that, thermohaline mixing is expected to dilute the accreted SN material in the bulk of the mass of [GV2003] N on a time scale of  $\sim 10^7$  yr. Thereby, the enhanced abundances of the measured elements will be reduced by factor of several, making them comparable to those found in the majority of the few main sequence components of LMXBs for which pollution has been detected previously<sup>1</sup>.

## Bibliography

1. González Hernández, J. I. *et al.* Chemical abundances of the secondary star in the black hole X-ray binary V404 Cygni. *Astrophys. J.* **738**, 95 (2011).
2. Filippenko, A. V. *et al.* Supernovae 2001co, 2003H, 2003dg, and 2003dr. IAU Circ. **8159**, 2 (2003).
3. Kasliwal, M. M. *et al.* Calcium-rich gap transients in the remote outskirts of galaxies. *Astrophys. J.* **755**, 161 (2012).
4. Kawabata, K. S. *et al.* A massive star origin for an unusual helium-rich supernova in an elliptical galaxy. *Nature* **465**, 326–328 (2010).
5. Waldman, R. *et al.* Helium shell detonations on low-mass white dwarfs as a possible explanation for SN 2005E. *Astrophys. J.* **738**, 21 (2011).
6. Moriya, T. *et al.* Fallback supernovae: a possible origin of peculiar supernovae with extremely low explosion energies. *Astrophys. J.* **719**, 1445–1453 (2010).
7. Sana, H. *et al.* Binary interaction dominates the evolution of massive stars. *Science* **337**, 444–446 (2012).
8. Chini, R., Hoffmeister, V. H., Nasser, A., Stahl, O., & Zinnecker, H. A spectroscopic survey on the multiplicity of high-mass stars. *Mon. Not. R. Astron. Soc.* **424**, 1925–1929 (2012).
9. Langer, N. Presupernova evolution of massive single and binary stars. *Ann. Rev. Astron. Astrophys.* **50**, 107–164 (2012).
10. Podsiadlowski, P., Joss, P. C. & Hsu, J. J. L. Presupernova evolution in massive interacting binaries. *Astrophys. J.* **391**, 246–264 (1992).
11. Lyman, J. *et al.* Bolometric light curves and explosion parameters of 38 stripped-envelope core-collapse supernovae. *Mon. Not. R. Astron. Soc.* **457**, 328–350 (2016).
12. Bhadkamkar, H. & Ghosh, P. Young pre-low-mass X-ray binaries in the propeller phase. Nature of the 6.7-h periodic X-ray source 1E 161348–5055 in RCW 103. *Astron. Astrophys.* **506**, 1297–1307 (2009).
13. Heinz, S. *et al.* The youngest known X-Ray binary: Circinus X-1 and its natal supernova remnant. *Astrophys. J.* **779**, 171 (2013).
14. Dickel, J. R., Strom, R. G. & Milne D. K. The radio structure of the supernova remnant G315.4–2.3 (MSH 14-63). *Astrophys. J.* **546**, 447–454 (2001).
15. Whiteoak, J. B. Z. & Green, A. J. The MOST supernova remnant catalogue (MSC). *Astron. Astrophys. Supp.* **118**, 329–380 (1996).

16. Smith, R. C. The discovery of Balmer-filaments encircling SNR RCW 86. *Astron. J.* **114**, 2664–2670 (1997).
17. Gvaramadze, V. V. & Vikhlinin, A. A. Point X-ray sources in the SNR G315.4–2.30 (MSH 14-63, RCW 86). *Astron. Astrophys.* **401**, 625–630 (2003).
18. Meyer, D. M.-A., Langer, N., Mackey, J., Velázquez, P. F. & Gusdorf, A. Asymmetric supernova remnants generated by Galactic, massive runaway stars. *Mon. Not. R. Astron. Soc.* **450**, 3080–3100 (2015).
19. Mignani, R. P., Tiengo, A. & de Luca, A. Optical and X-ray observations of candidate isolated neutron stars in the G315.4-2.3 supernova remnant. *Mon. Not. R. Astron. Soc.* **425**, 2309–2312 (2012).
20. Sollerman, J., Ghavamian, P., Lundqvist, P. & Smith, R. C. High resolution spectroscopy of Balmer-dominated shocks in the RCW 86, Kepler and SN 1006 supernova remnants. *Astron. Astrophys.* **407**, 249–257 (2003).
21. Güdel, M. X-ray astronomy of stellar coronae. *Astron. Astrophys. Rev.* **12**, 71–237 (2004).
22. Pecaut, M. J. & Mamajek, E. E. Intrinsic colors, temperatures, and bolometric corrections of pre-main-sequence stars. *Astrophys. J. Supp.* **208**, 9 (2013).
23. Tognelli, E., Prada Moroni, P. G. & Degl’Innocenti, S. The Pisa pre-main sequence tracks and isochrones. A database covering a wide range of Z, Y, mass, and age values. *Astron. Astrophys.* **533**, A109 (2011).
24. Hills, J. G. The effects of sudden mass loss and a random kick velocity produced in a supernova explosion on the dynamics of a binary star of arbitrary orbital eccentricity - Applications to X-ray binaries and to the binary pulsars. *Astrophys. J.* **267**, 322–333 (1983).
25. Tutukov, A. & Yungelson, L. Evolution of massive close binaries. *Nauchnye Informatsii*, **27**, 70–85 (1973).
26. Asplund, M., Grevesse, N., Sauval, A.J. & Scott P. The chemical composition of the Sun. *Annu. Rev. Astron. Astrophys.* **47**, 481–17522 (2009).
27. D’Antona, F. & Mazzitelli, I. New pre-main-sequence tracks for  $M$  less than or equal to 2.5 solar mass as tests of opacities and convection model. *Astrophys. J. Supp.* **90**, 467–500 (1994).
28. Sukhbold, T., Ertl, T., Woosley, S. E., Brown, J. & Janka, H.-T. Core-collapse supernovae from 9 to 120 solar masses based on neutrino-powered explosions. *Astrophys. J.* **821**, 38 (2016).
29. Perets, H. B. *et al.* A faint type of supernova from a white dwarf with a helium-rich companion. *Nature* **465**, 322–325 (2010).

**Acknowledgements** Based on observations collected at the European Southern Observatory, Chile, under programmes 095.D-0061 and 385.D-0198(A). V.V.G. is grateful to M.G. Revnivtsev for useful discussions, and acknowledges support from the Russian Science Foundation grant 14-12-01096.

**Author Contributions** V.V.G. and N.L. led the project and the manuscript writing. V.V.G., N.L., L.F. and D.C.-J.B. wrote the telescope proposals. L.F. reduced the VLT/FORS2 spectra and performed the spectral analysis. S.J. and D.C.-J.B. performed and analyzed the radio observations. I.Y.G. performed the PSF photometry. J.G. and A.R. performed the GROND observations and the SED fitting. N.C. performed part of the absolute wavelength calibration of the VLT/FORS2 spectra and worked on the removal of the spatially variable  $H\alpha$  emission. T.M.T. performed the Monte Carlo simulations of SN explosions in binary systems. Figures were prepared by V.V.G., L.F., A.R. and T.M.T. All authors contributed to the interpretation of the data and commented on the manuscript.

**Author Information** Reprints and permissions information is available at [www.nature.com/reprints](http://www.nature.com/reprints). The authors declare that they have no competing financial interests. Correspondence and requests for materials should be addressed to V.V.G. (vgvaram@mx.iki.rssi.ru) or N.L. (nlanger@astro.uni-bonn.de).

**Figure 1** SNR RCW 86 and [GV2003] N. From the upper left clockwise: Molonglo Observatory Synthesis Telescope 843 MHz<sup>15</sup> image of RCW 86, Digital Sky Survey II red band image of an arc-like optical nebula in the south-west corner of RCW 86, and VLT/FORS2 and *Chandra* images of two point sources, [GV2003] N and [GV2003] S, in the centre of the optical arc (marked, respectively, by blue and magenta circles). White spots in the VLT/FORS2 image are due to saturation effect. The orientation of the images is the same. At the distance of RCW 86 of 2.3 kpc, 10 arcmin and 5 arcsec correspond to  $\approx 6.6$  and 0.05 pc, respectively.

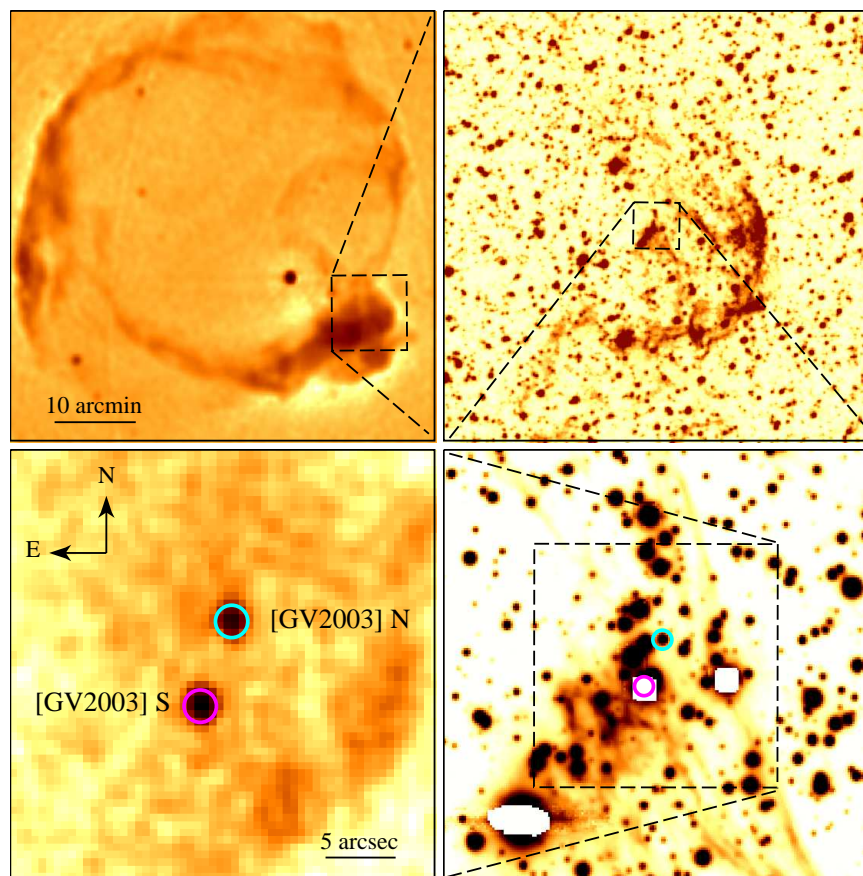


**Figure 2** Portion of the VLT/FORS2 spectrum of the optical counterpart of [GV2003]N. The observed spectrum (dots connected by a solid line) is compared with synthetic spectra calculated from the derived atmospheric parameters for the solar (red dashed line) and the final estimated abundances (blue solid line). The major components of each blend are labelled. One can see that the solar abundances are not a good match to the observed spectrum and that Ca and Fe are overabundant.

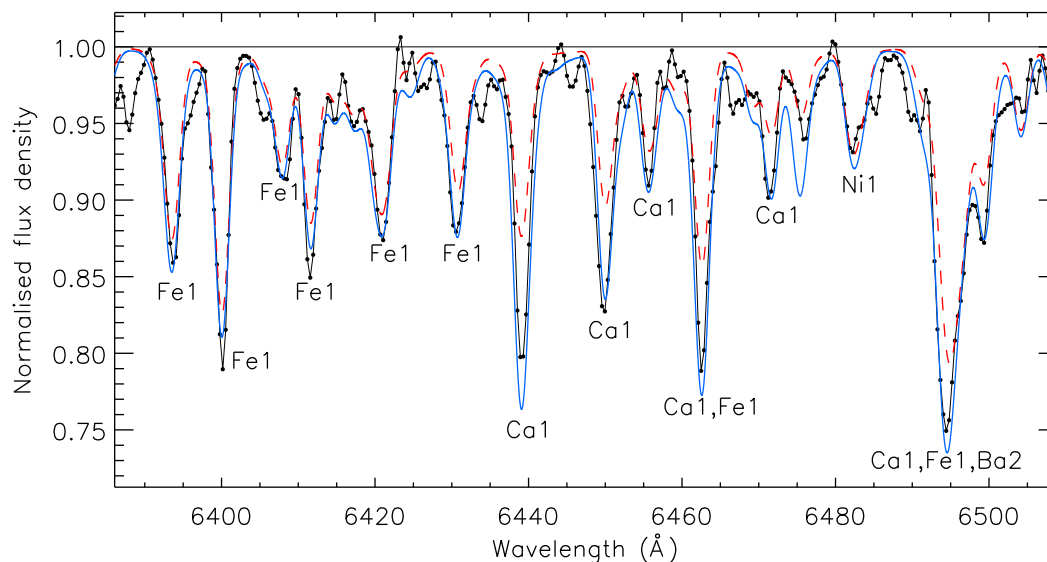
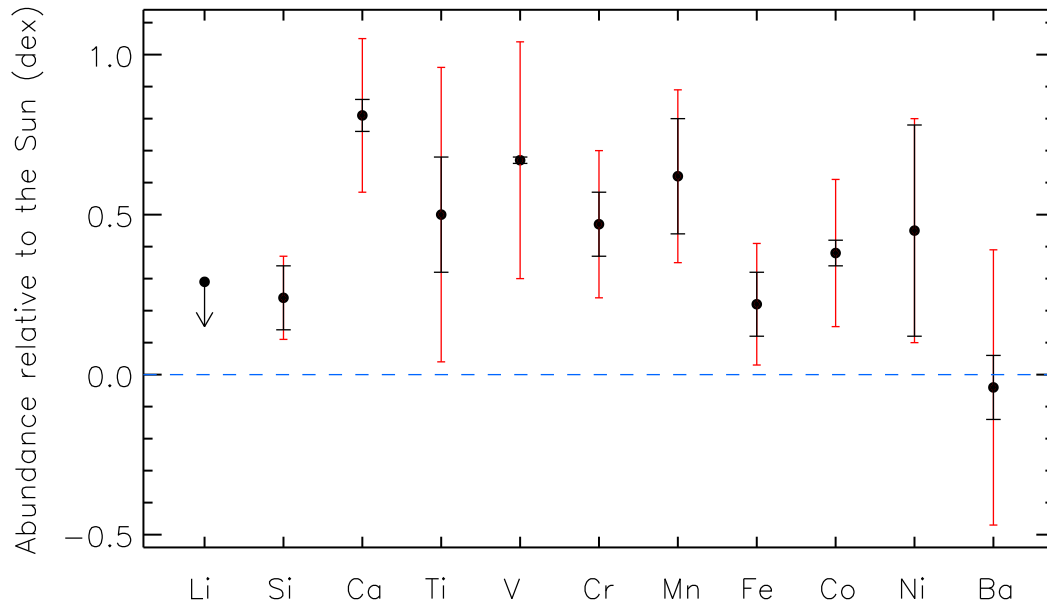




**Figure 3** Element abundances of the optical counterpart of [GV2003]N. The dashed line corresponds to solar abundance values. The smaller error bars indicate the statistical uncertainties, while the larger ones show the maximum systematic uncertainties. The real uncertainties lie in between. For the Li abundance we give only an upper limit. Note a very high overabundance of Ca.



## Methods

**Radio observations of [GV2003]N.** Observations were conducted in the L-band at the Parkes radio telescope on 2002 October 13. The bandwidth was 256 MHz, with 512 spectral channels. We observed [GV2003]N for about 7.5 hours, with a time resolution of 0.4 ms. The recorded data were dedispersed for 512 independent dispersion measures (DMs), uniformly spaced between zero and  $275 \text{ pc cm}^{-3}$ , beyond which the smearing of the signal in the individual spectral channels becomes greater than the sampling interval. Then, we searched for harmonically related peaks by the standard harmonic folding procedure, after performing a Fourier transform, for the time series corresponding to each DM. Details of statistically significant “candidates” were stored, and later used to produce coherently folded profiles for assessing the quality. The dedispersion of the data was performed with Taylor’s tree algorithm<sup>29</sup>, which assumes linearity of the dispersion delay as a function of frequency. In our case, the frequency was sufficiently high for the error due to this assumption to be negligible ( $\sim 1.2\%$ ), and we did not need to apply further correction to the band.

Ultimately, we did not detect any reliable (pulsed) radio signal from [GV2003]N, although our search was very sensitive. In general, detection sensitivity for pulsars is difficult to quantify, mainly because of uncertainties introduced by unknown duty cycle of pulsars, interstellar scattering, and the details of the search procedure. The sensitivity of our observations was estimated as follows. The telescope gain,  $G$ , of Parkes is  $\approx 0.65 \text{ K Jy}^{-1}$ . The system temperature,  $T_{\text{sys}}$ , in the L-band is  $\approx 32 \text{ K}$ , with a sky contribution of about 6 K. In general, one expects the intrinsic duty cycle of long period pulsars to be  $\sim 4\%$ . Interstellar scatter broadening and dispersion smearing will increase this width for high DM pulsars (these smearings add in quadrature with the pulse width). The minimum detectable flux can be written as  $S_{\text{min}} = (AT_{\text{sys}}/G)[w/(N_{\text{pol}}\beta T)(P - w)]^{1/2}$ , with  $A$ ,  $\beta$ ,  $N_{\text{pol}}$  and  $T$  being detection threshold in terms of r.m.s. of the noise, bandwidth, number of independent polarization channels, and total observation time, respectively. With a bandwidth of 256 MHz and observing time of 7.46 hrs ( $2^{26}$  samples at 0.4 ms intervals), this amounts to  $35 \mu\text{Jy}$  with a  $10\sigma$  limit. In comparison, this is about 3 times more sensitive than the Parkes Multi-beam Pulsar Survey<sup>30</sup>.

**VLT/FORS2 imaging of [GV2003]N.** [GV2003]N was observed with the Focal Reducer and low dispersion Spectrograph (FORS2) camera<sup>31</sup> at the ESO VLT in the  $V$  band on 2010 April 10–12. With the FORS2 resolution of 0.25 arcsec per pixel, we obtained high quality images from a total of 45 exposures of 300 s each in dark time, photometric conditions with seeing of  $\approx 0.6$  arcsec and an average airmass of  $\approx 1.3$ .

The image reduction was performed with the software package IRAF<sup>32</sup>. We created master bias and master normalized sky flat field calibration images. Detector bad pixel map was constructed from the ratio of low and high-count rate flats. These calibration products were used to process each individual  $V$ -band exposure. Single images were registered to a reference frame with the smallest airmass. Geometric transformation solutions were estimated with GEOMAP and GEOTRAN procedures using over a 1500 reference stars in common. The final average combined (with CCDCLIP algorithm) image was obtained from all images brought to the same zero (sky) level as

the reference using the mode value of a  $25 \text{ pixel} \times 25 \text{ pixel}$  statistics region. The large number of single exposures and the 9-point observing dither pattern allowed us to create a high S/N final average combined image, clean from remaining detector cosmetics (bad pixels and rows/columns) and cosmic ray hits. The full-width at half maximum (FWHM) of this image is 2.1 pixels, i.e. 0.53 arcsec.

We performed a point spread function (PSF) photometry on all sources in the final combined image. For that we created a PSF model using 168 isolated stars (no contaminating sources within a radius of 3 FWHM). Best photometry was obtained from a second order variable PSF model dependent on the position on the detector, resulting in negligible ( $<1\%$  in flux) residuals. The aperture and PSF photometry radius was chosen to be  $\sim 3 \text{ FWHM} \approx 6$  pixels, where the sky value was estimated locally from an annulus with a width of 5 pixels. Aperture correction to the PSF magnitudes was estimated from comparison between the PSF and aperture magnitudes of the isolated PSF stars used to build the PSF model. We perform PSF fitting photometry to all sources with detection threshold of  $4\sigma$  above the background. Optical counterpart to [GV2003]N was readily detected (see Fig. 1).

Photometric Stetson standard star fields of NGC 2437 and E5 (with 53 and 75 stars, respectively) were taken at the beginning and end of each night. These were used to obtain the photometric zeropoint ( $V_{\text{ZP}} = 28.1563 \pm 0.0013 \text{ mag}$ ) and airmass coefficients ( $X_V = 0.1996 \pm 0.0014 \text{ mag}$ ) to convert from instrumental to standard magnitudes. The aperture corrected instrumental PSF magnitudes were calibrated using these coefficients at an airmass of 1.269. We found that the apparent  $V$ -band magnitude of [GV2003]N is  $20.688 \pm 0.024$ .

**GROND photometry and SED fitting.** [GV2003]N was observed on 2013 April 8 simultaneously in 4 optical ( $g', r', i', z'$ ) and 3 near-infrared ( $J, H, K_s$ ) bands with the GROND instrument<sup>33</sup> at the 2.2 m MPG telescope at the ESO La Silla Observatory (Chile). Five exposures were obtained with combined integration of  $\approx 41$  min in the optical bands and  $\approx 53$  min in the near-infrared bands. Observing conditions were good with a medium seeing of 1 arcsec and an average airmass of 1.2. The data reduction was performed using standard IRAF tasks<sup>32,34</sup>. The  $g', r', i', z'$  photometry was obtained using PSF fitting while due to the undersampled PSF in the near-infrared, the  $J, H, K_s$  photometry was measured from apertures with the sizes corresponding to the FWHM of field stars. Calibration of the optical photometry was obtained using an observation of the same field obtained in a different night under photometric conditions and calibrated against an observation of an SDSS field<sup>35</sup>. Photometric calibration of the near-infrared bands was achieved against selected 2MASS<sup>36</sup> stars in the field of the target. The resulting AB magnitudes are:  $r' = 19.60 \pm 0.05 \text{ mag}$ ,  $i' = 18.77 \pm 0.08 \text{ mag}$ ,  $z' = 18.29 \pm 0.06 \text{ mag}$ ,  $J = 17.60 \pm 0.17 \text{ mag}$ ,  $H = 17.24 \pm 0.14 \text{ mag}$ , and  $K_s = 17.57 \pm 0.18 \text{ mag}$ . Using the LePHARE simulation program<sup>37</sup> and the NextGen model atmosphere grid<sup>38</sup>, and leaving the foreground reddening towards the source as a free parameter, we found that the best fitting SED ( $\chi^2 = 2.0$ ; Extended Data Fig. 1) is that of a star with an effective temperature of  $T_{\text{eff}} \approx 5200 \text{ K}$  and a colour excess of  $E(B - V) \approx 0.9 \text{ mag}$ .

**VLT/FORS2 spectroscopy of [GV2003]N.** [GV2003]N was observed once each night on 2015 April 14, 21, May 13 and 16 with the VLT/FORS2 instrument. The observations were conducted using a long slit with 1.0 arcsec width centred on the target. We used the 1200R grism in order to obtain a continuous coverage of the  $\approx 5870\text{--}7370\text{ \AA}$  wavelength range with an average spectral resolution, measured using the emission lines of the wavelength calibration lamps, of  $\Delta\lambda/\lambda \approx 2900$ . Each exposure was 2700 s long. For the parameter determination and abundance analysis, the four spectra have been co-added yielding a S/N per pixel of  $\approx 93$  at  $\approx 6800\text{ \AA}$ . The science images were reduced using a set of ten bias and ten flat-field images collected on the morning following each observing night. Each spectrum was extracted using an aperture of 12 pixels and by applying background subtraction. The spectra were wavelength calibrated using a wavelength calibration lamp obtained on the morning following each observing night. We further refined the absolute wavelength calibration using the sky Na I  $\lambda\lambda 5890, 5896$  emission lines, with a typical correction of  $\approx 2\text{ km s}^{-1}$ .

In order to derive an accurate RV from each spectrum of the star, we co-added the spectral lines using the Least-Squares Deconvolution technique (LSD), which is effective also with FORS spectra obtained with the 1200 grisms<sup>39</sup>. The LSD technique<sup>40</sup> combines line profiles centred at the position of the individual lines given in the line mask and scaled according to the line strength. The resulting average profiles were obtained by combining about 300 lines, yielding a strong increase in S/N, therefore improving the precision of the RV measurements. We prepared the line mask used by the LSD code, adopting the stellar temperature derived from the GROND SED, a surface gravity of  $10^{4.5}$  typical of main-sequence solar-like stars, and solar abundances<sup>26</sup>. We note that the FORS2 spectrum does not cover strong enough lines of two ionization stages of the same element to spectroscopically infer the surface gravity. We extracted the line parameters from the Vienna Atomic Line Database (VALD; ref.<sup>41</sup>) using all lines stronger than 20% of the continuum, avoiding hydrogen lines and lines in spectral regions affected by the presence of telluric and nebular features.

The RV values, obtained by fitting a Gaussian to each LSD profile, are listed in Table 1. The results show the presence of clear RV variations, indicative of binarity, with a period of the order of about a month, or less. The large RV variation derived from the two observations conducted in May, in contrast to that obtained from the April data on a similar time-base, is suggestive of an eccentric orbit, which is typical of young post-SN binaries<sup>24</sup>.

**Spectral analysis.** Because of the moderate resolution and hence strong line blending, the spectrum of [GV2003]N could be analyzed only through spectral synthesis. We calculated synthetic spectra with SYNTH3<sup>42</sup> on the basis of line lists extracted from the VALD database and of model atmospheres calculated with the LLMODELS stellar model atmosphere code<sup>43</sup>. For all calculations we assumed Local Thermodynamical Equilibrium (LTE), plane-parallel geometry, and a microturbulence velocity of  $1.0\text{ km s}^{-1}$ , typical of solar-like stars (e.g. ref.<sup>44</sup>).

The effective temperature of solar-like stars can be best estimated using the wings of hydrogen lines,  $H\alpha$  in particular<sup>45</sup>, which is fully covered by the FORS2 spectra. Unfortunately, the intensity of the nebular  $H\alpha$  emission varies strongly in the region around [GV2003]N, preventing

a reliable background subtraction at the wavelengths covered by the  $H\alpha$  line. We therefore derived  $T_{\text{eff}}$  from the analysis of the Fe I lines. We selected a set of 15 strong and weakly blended Fe I lines from which we derived the iron abundance<sup>46</sup>. By imposing no correlation between line abundance and excitation energy and taking into account the results obtained from the SED, we estimated an effective temperature of  $5100 \pm 200$  K. The broadening of the spectral lines is dominated by the instrumental resolution; this sets an upper limit on the stellar projected rotational velocity  $v \sin i$  of about  $80 \text{ km s}^{-1}$ . Because of the lack of spectroscopic  $\log g$  indicators, we adopted the stellar surface gravity obtained from comparing the position of the star in the HertzsprungRussell diagram with evolutionary tracks, as described in the main text.

On the basis of the derived stellar parameters, we derive the abundance of Si, Ca, Ti, V, Cr, Mn, Fe, Co, Ni, and Ba (Fig 3). Because of the rather large overabundances, we followed the same procedure typically adopted for a self-consistent analysis of magnetic chemically peculiar stars, hence iteratively re-calculating a new grid of model atmosphere, atmospheric parameters, and abundances each time the abundances changed significantly from the previous iteration<sup>47</sup>. This was possible because the model atmosphere code allows the use of individualized abundance patterns.

After convergence, we derived the statistical abundance uncertainty for each element, i.e., the standard deviation from the average abundance given a set of two or more lines, and the maximum systematic uncertainty, which takes into account the error bars on the atmospheric parameters: 200 K for  $T_{\text{eff}}$ , 0.1 dex for  $\log g$ , and  $0.5 \text{ km s}^{-1}$  for the microturbulence velocity. The statistical uncertainty accounts for uncertainties in the placement of the continuum and in the atomic data. For the elements for which we derived the abundance from one line, we assumed that the statistical uncertainty is equal to that of Fe. The true uncertainty lies in between the statistical and maximum systematic uncertainties<sup>48</sup>.

The spectrum does not show the presence of the Li I  $\lambda 6708 \text{ \AA}$  line; we could therefore derive an upper limit on the Li abundance. The Mn and Ba abundances were derived taking into account hyperfine structure. The resulting abundances for all considered elements are listed in Extended Data Table 2.

## Bibliography

29. Taylor, J. H. A sensitive method for detecting dispersed radio emission. *Astron. Astrophys. Supp.* **15**, 367–369 (1974).
30. Manchester, R. N. *et al.* The Parkes multi-beam pulsar survey – I. Observing and data analysis systems, discovery and timing of 100 pulsars. *Mon. Not. R. Astron. Soc.* **328**, 17–35 (2001).
31. Appenzeller, I. *al.* Successful commissioning of FORS1 – the first optical instrument on the VLT. *Messenger* **94**, 1–6 (1998).
32. Tody, D. IRAF in the nineties. *Astronomical Data Analysis Software and Systems II* (eds Hanisch, R. J., Brissenden, R. J. V. & Barnes, J.) 173–183 (ASP Conf. Ser. 52, 1993).

33. Greiner, J. *et al.* GROND – a 7-channel imager. *Pub. Astron. Soc. Pac.* **120**, 405–424 (2008).
34. Krühler, T. *et al.* The 2175 Å feature in a gamma-ray burst afterglow at redshift 2.45. *Astrophys. J.* **685**, 376–383 (2008).
35. Aihara, H. *et al.* The eighth data release of the Sloan Digital Sky Survey: First data from SDSS-III. *Astrophys. J. Supp.* **193**, 29 (2011).
36. Skrutskie, M. F. *et al.* The Two Micron All Sky Survey (2MASS). *Astron. J.* **131**, 1163–1183 (2006).
37. Arnouts, S. & Ilbert, O. Le PHARE: Photometric analysis for redshift estimate. <http://www.cfht.hawaii.edu/~arnouts/LEPHARE> (2014).
38. Hauschildt, P. H., Allard, F. & Baron E. The NextGen model atmosphere grid for  $3000 \leq T_{\text{eff}} \leq 10,000$  K. *Astrophys. J.* **512**, 377–385 (1999).
39. Bagnulo, S., Landstreet, J. D., Fossati, L., & Kochukhov, O. Magnetic field measurements and their uncertainties: the FORS1 legacy. *Astron. Astrophys.* **538**, A129 (2012).
40. Kochukhov, O., Makaganiuk, V. & Piskunov, N. Least-squares deconvolution of the stellar intensity and polarization spectra. *Astron. Astrophys.* **524**, A5 (2010).
41. Piskunov, N. E., Kupka, F., Ryabchikova, T. A., Weiss, W. W. & Jeffery, C. S. VALD: The Vienna Atomic Line Data Base. *Astron. Astrophys. Supp.* **112**, 525–535 (1995).
42. Kochukhov, O. Spectrum synthesis for magnetic, chemically stratified stellar atmospheres. in *Physics of Magnetic Stars* (eds Romanyuk, I.I. & Kudryavtsev, D. O.) 109–118 (2007).
43. Shulyak, D., Tsymbal, V., Ryabchikova, T., Stütz, C. & Weiss, W. W. Line-by-line opacity stellar model atmospheres. *Astron. & Astrophys.* **428**, 993–1000 (2004).
44. Bruntt, H. *et al.* Accurate fundamental parameters for 23 bright solar-type stars. *Mon. Not. R. Astron. Soc.* **405**, 1907–1923 (2010).
45. Fuhrmann, K., Axer, M., & Gehren, T. Balmer lines in cool dwarf stars. 1. Basic influence of atmospheric models. *Astron. & Astrophys.* **271**, 451–462 (1993).
46. Fossati, L. *et al.* Late stages of the evolution of A-type stars on the main sequence: comparison between observed chemical abundances and diffusion models for 8 Am stars of the Praesepe cluster. *Astron. & Astrophys.* **476**, 911–925 (2007).
47. Shulyak, D., Ryabchikova, T., Mashonkina, L., & Kochukhov, O. Model atmospheres of chemically peculiar stars. Self-consistent empirical stratified model of HD 24712. *Astron. & Astrophys.* **499**, 879–890 (2009).
48. Fossati, L. *et al.* The chemical abundance analysis of normal early A- and late B-type stars. *Astron. & Astrophys.* **503**, 945–962 (2009).

## Supplementary Information

### 1. RCW 86 as the result of a SN explosion near the edge of a wind-blown bubble

RCW 86 (also G315.4–2.30, MSH 14–63) is a young Galactic shell-like SNR with an angular diameter of about  $40'$ , which – for a distance to the remnant of 2.3 kpc (ref.<sup>20</sup>) – corresponds to  $\approx 26$  pc. The almost complete shell of RCW 86, visible in X-ray<sup>49</sup>, optical<sup>16</sup>, radio<sup>15</sup> and infrared<sup>50</sup> wavelengths, has a bright peculiar protrusion to the south-west, what gives the SNR a pyriform appearance (see fig. 6 in ref.<sup>16</sup>). At optical wavelengths, the protrusion appears as a ragged arc-like nebula<sup>51,52</sup> (Fig. 1) with a radius of about  $2'$  (1.1 pc). Spectroscopic observations of the arc indicate that the SN blast wave expands with a velocity of  $\sim 100 \text{ km s}^{-1}$  at this location. Deep imaging of RCW 86 revealed that almost the whole periphery of the SNR is encompassed by Balmer-dominated filaments<sup>16</sup>. Spectra of these filaments indicate shock velocities of  $\approx 500 - 900 \text{ km s}^{-1}$  (ref.<sup>20,53</sup>). Similar velocities of the SN blast wave were also inferred from observations of thermal X-ray emission in RCW 86<sup>49</sup>, while the detection of nonthermal X-ray emission in this SNR<sup>49,54,55</sup> implies the existence of shocks with even higher speeds. Recent proper motion measurement of a nonthermal X-ray filament in the north-east rim of RCW 86 showed<sup>56</sup> that the blast wave expands there with a speed of  $\approx 3000 \text{ km s}^{-1}$ .

The striking asymmetry in expansion velocity of the SN blast wave was interpreted as an indication that the SN explosion has occurred within a low-density bubble created by the wind of the progenitor star<sup>57</sup>, and that the actual SN explosion centre is closer to the south-west edge of the bubble because the ambient medium in this direction is denser than in the opposite (north-east) one<sup>58</sup>. Correspondingly, it was suggested that the SN blast wave has already hit the nearest (south-west) edge of the bubble and slowed down its velocity to  $\approx 600 \text{ km s}^{-1}$ , while in the opposite direction it still freely expands within the bubble. This scenario is widely accepted in subsequent papers<sup>50,59</sup> on RCW 86, in particular, to explain the young kinematic age of the SN blast wave implied by the possible association of this SNR with the historical supernova of A.D. 185 (SN 185)<sup>60</sup>.

Gvaramadze & Vikhlinin<sup>17</sup> supplemented the cavity explosion scenario by Vink et al.<sup>57</sup> by suggesting that the cavity was created by a moving star and that the SN explosion in RCW 86 has occurred near the edge of the cavity – in the centre of the south-west protrusion, which is similar to the model put forward by Wang et al.<sup>61</sup> to explain the origin of large-scale structures (in particular the Napoleon's Hat) around the SN 1987A. An interesting consequence of this interpretation is that after the blast wave will have completely overrun the south-west protrusion, RCW 86 will assume a two-shell form, with a newly-formed shell attached to the already existing one. This points to the possibility that some of the known two-shell SNRs could originate from off-centred cavity SN explosions<sup>62</sup>.

Including our results, we arrive at the following scenario. The SN progenitor was a  $\sim 10 M_{\odot}$  star in a tight binary system with a low-mass companion and the SN explosion was of Type Ib. This means that before the SN explosion the binary system has lost a significant fraction of its initial mass,  $M_i$ , through a common-envelope ejection. The ejected mass is expected to be about  $5 M_{\odot}$ , since (single)  $10 M_{\odot}$  stars lose only about 10% of  $M_i$  during their lives, and the pre-SN mass of

the exploding star is constrained to  $\leq 4 M_{\odot}$ . After the common-envelope ejection, the stripped star could still be surrounded by a thin hydrogen envelope<sup>63</sup>, which is blown off later on through a fast line-driven wind. This wind would sweep-up the material of the common-envelope ejecta in a dense shell, which we now observe as an arc-like nebula in the south-west corner of RCW 86.

From the expected ejection velocity of the common envelope of several tens of  $\text{km s}^{-1}$  and given the radius of the optical arc of  $\approx 1.1$  pc, one finds that the envelope ejection event occurred a few  $10^4$  yr before the SN explosion. This time-scale is similar to the duration of the shell helium burning phase of  $\sim 10 M_{\odot}$  stars<sup>64</sup>, which implies that a case C Roche-lobe overflow initiated the common envelope evolution. Using the number density of the local interstellar medium of  $\sim 0.5 \text{ cm}^{-3}$  (ref.<sup>50</sup>), one finds that the common-envelope ejecta so far swept-up only  $\sim 0.1 M_{\odot}$  of the ambient gas, which in turn implies that the arc should be composed mostly of the material lost by the binary system, and that it should therefore be overabundant in nitrogen by a factor of three or so<sup>65</sup>. Optical spectroscopy of filaments at several positions in the optical arc revealed<sup>66</sup> a factor of two overabundance of nitrogen with respect to the value typical of old Galactic SNRs. Although this overabundance is slightly lower than what is expected from our scenario, we note that the observed spectra could be a superposition of spectra produced in regions with different physical conditions (e.g. because of the presence of shocks with different velocities along the same line-of-sight), which makes it difficult to determine the nitrogen and other chemical abundances with standard methods (cf. ref.<sup>66</sup>).

## 2. Chemical abundances in LMXBs

Heavy element enrichment due to an exploding binary companion have been measured in a handful of stars<sup>1,67–69</sup>, all in active X-ray binaries, where the X-rays produced by mass transfer from a low mass main sequence star to a compact companion prove the physical connection of both components. Except for one object (Nova Scorpius), the pollution of the low mass star with SN products is rather mild, i.e., some metal abundances are typically enhanced by a factor of two, with an oxygen enhancement of ten in Nova Scorpius as the record holder<sup>67</sup>. Remarkably, the Ca overabundances of all objects so far are smaller than a factor of 1.6, including that in Nova Scorpius (see table 5 in ref.<sup>1</sup>). This is to be contrasted with the Ca enhancement of a factor of 6 in [GV2003] N.

More importantly, in the known post-SN binaries Si is more overabundant than Ca<sup>1</sup>. This is consistent with studies<sup>70,71</sup> of explosive yields from (single) stars with  $M_i \geq 11 M_{\odot}$ , which show that Si is generally produced in larger amounts than Ca. While, in principle, selective accretion could still lead to the observed abundance pattern in [GV2003] N, we consider this unlikely since the velocities of the Ca- and Si-rich layers in the ejecta of a normal core-collapse SN are similar. We suggest therefore that the elevated overabundance of Ca with respect to Si is intrinsic to the SN ejecta, which points to the possibility that RCW 86 is the result of a Ca-rich SN explosion (see next section).

## 3. Calcium-rich SNe



Ca-rich SNe are a recently defined class of faint and rapidly evolving SNe whose observational properties appear challenging to explain. While at maximum light, the optical spectra resemble those of Type Ib SNe, thus showing lines of helium but not of hydrogen<sup>3</sup>, these objects quickly evolve to the optically thin nebular phase (at  $\sim 2$  months), where their optical spectra are dominated by [Ca II], with lines from oxygen or other intermediate mass elements being weak or absent.

The question which progenitors can produce Ca-rich SNe is not settled. These SNe appear to occur in early type galaxies and many of them are found at large (up to 150 kpc) galactocentric distances<sup>72,73</sup>. This points towards relatively large progenitor lifetimes (from tens to hundreds of Myr) and/or very high ( $\sim 1000 \text{ km s}^{-1}$ ) space velocities<sup>73</sup>, which in turn implies low-mass SN progenitor stars. However, a fraction of the Ca-rich SNe are found within their host galaxies<sup>74</sup> and many of the host galaxies show signs of galaxy-galaxy interaction or merger<sup>4,73</sup>. The latter implies that the host galaxies of the Ca-rich SNe might be sites of recent (massive) star formation and that some of these SNe might originate from massive stars. Correspondingly, thermonuclear events from white dwarf progenitors<sup>5,29,75,76</sup> and core-collapse events produced from stripped low-mass ( $M_i \sim 10 M_\odot$ ) massive stars<sup>4,6</sup> have been proposed to explain the Ca-rich SNe. In both cases, explosive helium burning is expected to occur. Whereas SN simulations of stripped stars are available only for stars with rather large  $M_i$  (e.g. ref.<sup>77</sup> and references therein), Waldman et al.<sup>5</sup> found in simulations of helium shell detonations on CO white dwarfs that Ca may be the most abundant product in such events, together with large amounts of unburnt helium.

In parameterized explosive helium burning conditions, Hashimoto et al.<sup>78</sup> find Ca to be the main product for a peak temperature of  $\approx 1.3 \times 10^9 \text{ K}$ . Assuming the core radius of a white dwarf of  $r = 0.01 R_\odot$  and adopting the SN post-shock temperature  $T_{\text{ps}} = [3E_{\text{SN}}/(4\pi r^3 a)]^{1/4}$  from ref.<sup>79</sup>, with  $E_{\text{SN}}$  being the SN kinetic energy and  $a = 7.57 \times 10^{-15} \text{ erg cm}^{-3} \text{ K}^{-4}$  being the radiation constant, one finds that  $T_{\text{ps}}$  would reach the above value if  $E_{\text{SN}} = 3 \times 10^{49} \text{ erg}$ . Weaver & Woosley<sup>79</sup> argue for a shock-induced production of Ca at somewhat higher temperature of  $T_{\text{ps}} \approx 3.5 \times 10^9 \text{ K}$ , which would require  $E_{\text{SN}} \sim 10^{51} \text{ erg}$ . In the lowest mass stripped core-collapse SN progenitors, the mass of the mantle of intermediate mass elements surrounding the innermost strongly electron-degenerate core is extremely small<sup>64,80</sup>. Thus the massive helium shell — which is strongly diminished in single stars due to the second dredge-up<sup>81</sup>, but which remains intact in stripped stars — is located at a very small radius and can therefore be exposed to very high temperatures when the SN shock wave passes through. It thus appears possible, but remains to be shown with detailed models, that SNe from stripped stars of relatively low  $M_i$  produce fast and faint transients with Ca- and helium-rich ejecta. This possibility is supported by the finding that the light curves produced by stripped electron-capture SNe are consistent with those of the Ca-rich SNe<sup>82</sup>.

#### 4. Simulated effects of a SN explosion in a tight binary

We performed Monte Carlo calculations of 10 000 asymmetric SN explosions to simulate the resulting kinematics on the surviving binary system containing a NS and a  $0.9 M_\odot$  G-dwarf, based on the equations of Tauris & Takens<sup>83</sup>. The impact of the SN shell is modelled according to the three-dimensional hydrodynamical simulations results of Liu et al.<sup>84</sup>, by applying their power-law

fit (see their fig. 6) for a  $0.9 M_{\odot}$  main-sequence companion star which experiences shell impact from a nearby, stripped exploding core of  $3.0 M_{\odot}$ .

The mass of the exploding star and the pre-SN orbital period are randomly drawn from the intervals  $2.9 - 3.7 M_{\odot}$  and  $0.28 - 1.0$  d. The chosen mass interval corresponds to  $M_i$  in the range  $10 - 13 M_{\odot}$  (see main text). A minimum pre-SN orbital period of  $0.28$  d was adopted to prevent the  $0.9 M_{\odot}$  star from filling its Roche lobe, which would most likely lead to a merger event. The upper limit of the orbital period is given by the strong pollution of the companion star with heavy elements from the SN ejecta, which means that the pre-SN orbit must have been tight. The momentum kicks are randomly drawn from the range of  $0 - 500 \text{ km s}^{-1}$ , assuming an isotropic distribution of kick directions. We assume a NS with a mass of  $1.4 M_{\odot}$  is formed, releasing a gravitational binding energy of  $0.16 M_{\odot} c^2$  (ref.<sup>85</sup>). Since we estimate a post-SN orbital period in the range of  $10 - 30$  d (Methods) we consider only cases where this is achieved.

Extended Data Fig. 2 (left panel) shows that the most likely obtained systemic velocities are of the order of  $80 \text{ km s}^{-1}$ , in agreement with observational constraints based on the location of the NS relative to the centre of the optical arc in the south-west of RCW 86. We found a minimum orbital eccentricity of  $0.7$ . Liu et al.<sup>84</sup> obtained the mass of accreted SN ejecta by the companion star as function of  $E_{\text{SN}}$  and the pre-SN binary separation. We parameterized their results, and applied them to our calculations. Extended Data Fig. 2 (right panel) shows that using the canonical value of  $E_{\text{SN}} = 10^{51} \text{ erg}$  results in very small accreted amounts of SN ejecta (blue histogram, left), but a five times smaller SN energy yields values (red histogram, right) which are well compatible with the enrichments seen in [GV2003]N (see main text). A smaller than canonical supernova energy is also consistent with our initial mass estimate of the SN progenitor of about  $10 M_{\odot}$  (cf. ref.<sup>4,86</sup>).

## References

49. Borkowski, K. J., Lierly, W. J. & Reynolds, S. P. Supernova remnants in the Sedov expansion phase: Thermal X-Ray emission. *Astrophys. J.* **548**, 820–835 (2001).
50. Williams, B.J. *et al.* RCW 86: A type Ia supernova in a wind-blown bubble. *Astrophys. J.* **741**, 96 (2011).
51. Rodgers, A. W., Campbell, C. T. & Whiteoak, J. B. A catalogue of  $\text{H}\alpha$ -emission regions in the southern Milky Way. *Mon. Not. R. Astron. Soc.* **121**, 103–110 (1960).
52. Rosado, M., Ambrocio-Cruz, P., Le Coarer, E. & Marcelin, M. Kinematics of the galactic supernova remnants RCW 86, MSH 15-56 and MSH 11-61A. *Astron. Astrophys.* **315**, 243–252 (1996).
53. Long, K. S. & Blair, W. P. The identification of Balmer-dominated filaments in RCW 86. *Astrophys. J.* **358**, L13–L16 (1990).

54. Bamba, A., Koyama, K. & Tomida, H. Discovery of non-thermal X-rays from the shell of RCW 86. *Publ. Astron. Soc. Japan* **52**, 1157–1163 (2000).
55. Rho, J., Dyer, K., Borkowski, K. J. & Reynolds, S. P. X-Ray synchrotron-emitting Fe-rich ejecta in supernova remnant RCW 86. *Astrophys. J.* **581**, 1116–1131 (2002).
56. Yamaguchi, H. *et al.* The refined shock velocity of the X-Ray filaments in the RCW 86 north-east rim. *Astrophys. J.* **820**, L3 (2016).
57. Vink, J., Kaastra, J. S. & Bleeker, J. A. M. X-ray spectroscopy of the supernova remnant RCW 86. A new challenge for modeling the emission from supernova remnants. *Astron. Astrophys.* **328**, 628–633 (1997).
58. Vink, J., Bocchino, F., Damiani, F., & Kaastra, J. S. An unresolved X-ray source inside the supernova remnant RCW 86. *Astron. Astrophys.* **362**, 711–714 (2000).
59. Broersen, S., Chiotellis, A., Vink, J. & Bamba, A. The many sides of RCW 86: a Type Ia supernova remnant evolving in its progenitor’s wind bubble. *Mon. Not. R. Astron. Soc.* **441**, 3040–3054 (2014).
60. Clark, D. H. & Stephenson, F. R. The remnants of the supernovae of AD 185 and AD 393. *Observatory* **95**, 190–195 (1975).
61. Wang, L., Dyson, J. E. & Kahn, F. D. The nature of the Napoleon’s Hat nebula of SN 1987A. *Mon. Not. R. Astron. Soc.* **261**, 391–395 (1993).
62. Gvaramadze, V. V. On the origin of two-shell supernova remnants. *UV Astronomy: Stars from Birth to Death* (eds Gomez de Castro A. I. & Barstow M. A.) 205–210 (2007).
63. Yoon, S.-C., Woosley, S. E. & Langer, N. Type Ib/c supernovae in binary systems. I. Evolution and properties of the progenitor stars. *Astrophys. J.* **725**, 940–954 (2010).
64. Jones, S. *et al.* Advanced burning stages and fate of 8 – 10  $M_{\odot}$  stars. *Astrophys. J.* **772**, 150 (2013).
65. Brott, I. *et al.* Rotating massive main-sequence stars. I. Grids of evolutionary models and isochrones. *Astron. Astrophys.* **530**, A115 (2011).
66. Ruiz, M. T. Spectroscopy of RCW 86 - A young supernova remnant. *Astrophys. J.* **243**, 814–816 (1981).
67. Israelian, G., Rebolo, R., Basri, G., Casares, J. & Martin, E. L. Evidence of a supernova origin for the black hole in the system GRO J1655–40. *Nature* **401**, 142–144 (1999).
68. González Hernández, J. I. *et al.* P. Chemical abundances in the secondary star of the neutron star binary Centaurus X-4. *Astrophys. J.* **630**, 495–505 (2005).

69. Suárez-Andrés, L., González Hernández, J. I., Israelian, G., Casares, J. & Rebolo, R. Chemical abundances of the secondary star in the neutron star X-ray binary Cygnus X-2. *Mon. Not. R. Astron. Soc.* **447**, 2261–2273 (2015).
70. Chieffi, A. & Limongi, M. Pre-supernova evolution of rotating solar metallicity stars in the mass range 13 – 120  $M_{\odot}$  and their explosive yields. *Astrophys. J.* **764**, 21 (2013).
71. Woosley, S. E. & Weaver, T. A. The evolution and explosion of massive stars. II. Explosive hydrodynamics and nucleosynthesis. *Astrophys. J. Supp.* **101**, 181–235 (1995).
72. Lyman, J. D., Levan, A. J., Church, R. P., Davies, M. B. & Tanvir, N. R. The progenitors of calcium-rich transients are not formed in situ. *Mon. Not. R. Astron. Soc.* **444**, 2157–2166 (2014).
73. Foley, R. J. Kinematics and host-galaxy properties suggest a nuclear origin for calcium-rich supernova progenitors. *Mon. Not. R. Astron. Soc.* **452**, 2463–2478 (2015).
74. Lyman, J. D. *et al.* N. R. Hubble Space Telescope observations of the host galaxies and environments of calcium-rich supernovae. *Mon. Not. R. Astron. Soc.* **458**, 1768–1777 (2016).
75. Shen, K. J. & Bildsten, L. Unstable helium shell burning on accreting white dwarfs. *Astrophys. J.* **699**, 1365–1373 (2009).
76. Sell, P. H., Maccarone, T. J., Kotak, R., Knigge, C. & Sand, D. J. Calcium-rich gap transients: tidal detonations of white dwarfs? *Mon. Not. R. Astron. Soc.* **450**, 4198–4206 (2015).
77. Dessart, L. *et al.* Inferring supernova IIb/Ib/Ic ejecta properties from light curves and spectra: correlations from radiative-transfer models. *Mon. Not. R. Astron. Soc.* **458**, 1618–1635 (2016).
78. Hashimoto, M.-A., Hanawa, T. & Sugimoto, D. Explosive helium burning at constant pressures. *Publ. Astron. Soc. Japan* **35**, 1–15 (1983).
79. Weaver, T. A. & Woosley, S. E. Evolution and explosion of massive stars. *Annals of the New York Academy of Sciences* **336**, 335–357 (1980).
80. Wanajo, S., Nomoto, K., Janka, H.-T., Kitaura, F. S. & Müller, B. Nucleosynthesis in electron capture supernovae of asymptotic giant branch stars. *Astrophys. J.* **695**, 208–220 (2009).
81. Podsiadlowski, P. *et al.* The effects of binary evolution on the dynamics of core collapse and neutron star kicks. *Astrophys. J.* **612**, 1044–1051 (2004).
82. Moriya, T. J. & Eldridge, J. J. Rapidly-evolving faint transients from stripped-envelope electron-capture supernovae. *Mon. Not. R. Astron. Soc.* **461**, 2155–2161 (2016).
83. Tauris, T. M. & Takens, R. J. Runaway velocities of stellar components originating from disrupted binaries via asymmetric supernova explosions. *Astron. Astrophys.* **330**, 1047–1059 (1998).

84. Liu Z.-W. *et al.* The interaction of core-collapse supernova ejecta with a companion star. *Astron. Astrophys.* **584**, A11 (2015).
85. Lattimer, J. M. & Yahil, A. Analysis of the neutrino events from supernova 1987A., *Astrophys. J.* **340**, 426–434 (1989).
86. Tauris, T. M., Langer, N. & Podsiadlowski, P. Ultra-stripped supernovae: progenitors and fate. *Mon. Not. R. Astron. Soc.* **451**, 2123–2144 (2015).

**Figure 4** Extended Data Figure 1 **Observed spectral energy distribution of [GV2003]N.** Data points (filled red circles) show the GROND  $g'r'i'z'JHK_K$  magnitudes. The horizontal error bars represent the full-width at half maximum of the GROND filters. The quadratic sum of the statistical uncertainties and the systematic uncertainties of the brightness measurement are shown as vertical error bars (in most cases they are within the size of the data points). The best fitting spectral energy distribution (solid line) is that of a star with an effective temperature of  $\approx 5200$  K and the colour excess of  $E(B - V)=0.9$  mag.

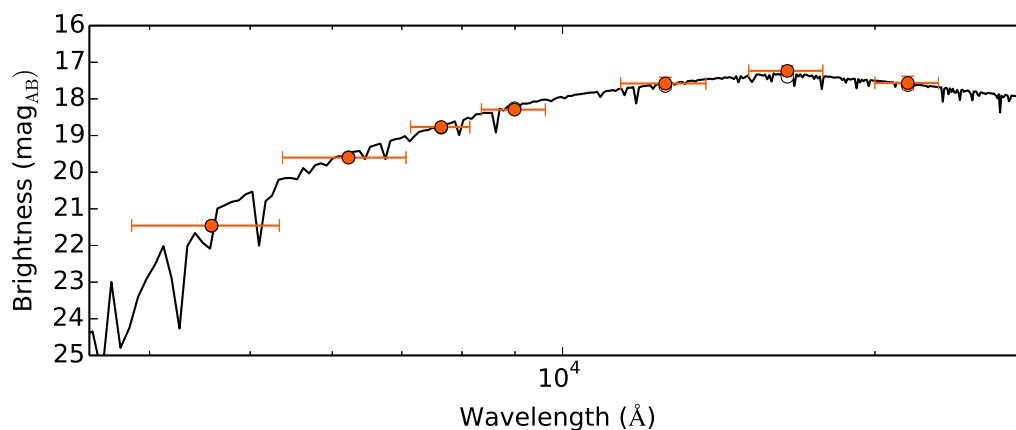


**Figure 5** **Extended Data Figure 2** **Results of simulations of 10,000 asymmetric SNe in tight binary systems.** The binary systems were assumed to be composed of an exploding  $2.9 - 3.7 M_{\odot}$  core and a  $0.9 M_{\odot}$  main sequence star with an orbital period between 0.28 and 1.0 d. Kick velocities were chosen randomly in the range from 0 to  $500 \text{ km s}^{-1}$ . The left panel shows the resulting systemic velocities of the post-SN binaries. The right panel gives the amount of SN ejecta accreted by the main sequence star, calculated for two values of the SN kinetic energy:  $E_{SN} = 10^{51} \text{ egr}$  (blue histogram, left) and  $E_{SN} = 2 \times 10^{50} \text{ egr}$  (red histogram, right).

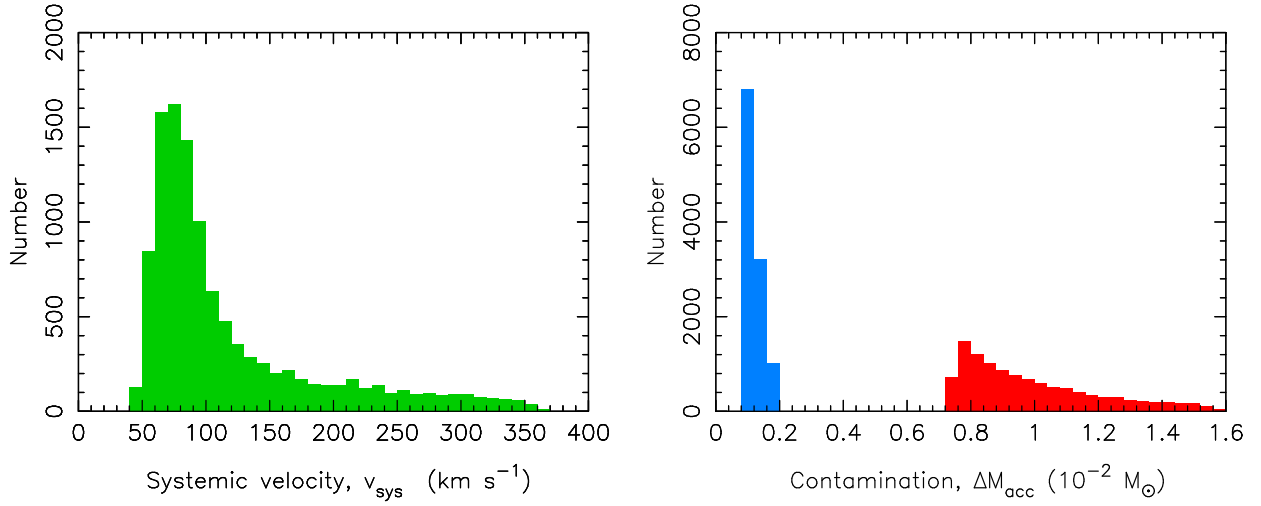


Table 1: **Radial velocity changes with time in the spectrum of [GV2003] N**

Date	Radial velocity* ( $\text{km s}^{-1}$ )	Heliocentric correction ( $\text{km s}^{-1}$ )
2015 April 14	$-71 \pm 2$	13.0
2015 April 21	$-74 \pm 4$	10.9
2015 May 13	$-44 \pm 3$	3.3
2015 May 16	$-62 \pm 3$	2.4

\* Corrected for the heliocentric motion of the Earth.

Table 2: **Extended Data Table 1 Surface element abundances of [GV2003] N**

Element	$X/H$	$M_{\text{acc}}/(10^{-5} M_{\odot})$
Li	$<0.29^*$	—
Si	$0.24 \pm 0.10(0.13)^{\dagger}$	8
Ca	$0.81 \pm 0.05(0.24)$	7
Ti	$0.50 \pm 0.18(0.46)$	0.09
V	$0.67 \pm 0.01(0.37)$	0.028
Cr	$0.47 \pm 0.10(0.23)$	0.6
Mn	$0.62 \pm 0.18(0.27)$	0.8
Fe	$0.22 \pm 0.10(0.19)$	15
Co	$0.38 \pm 0.04(0.23)$	0.09
Ni	$0.45 \pm 0.33(0.35)$	1.8
Ba	$-0.04 \pm 0.10(0.43)$	0

Abundances for elements are  $X/H = \log[N(X)/N(\text{H})]_{\text{star}} - \log[N(X)/N(\text{H})]_{\odot}$ , where  $N(X)$  is number density of atoms. In the third column we provide the implied amount of accreted mass per element assuming dilution in a convective envelope of  $0.2 M_{\odot}$ .

\* For the Li abundance only an upper limit is derived (see Methods).

$\dagger$  The uncertainties quoted for the abundances are statistical and maximum systematic (in brackets). The true uncertainties lie in between.